

# Room temperature dynamic correlation between methylammonium molecules in lead-iodine based perovskites: An *ab-initio* molecular dynamics perspective

Jonathan Lahnsteiner,<sup>1</sup> Georg Kresse,<sup>1</sup> Abhinav Kumar,<sup>2</sup> D.D. Sarma,<sup>2</sup> Cesare Franchini,<sup>1</sup> and Menno Bokdam<sup>1,\*</sup>

<sup>1</sup>*University of Vienna, Faculty of Physics and Center for Computational Materials Science, Sensengasse 8/12, A-1090 Vienna, Austria*

<sup>2</sup>*Solid State and Structural Chemistry Unit, Indian Institute of Science, 560012 Bangaluru, India*

(Dated: November 7, 2018)

The high efficiency of lead organo-metal-halide perovskite solar cells has raised many questions about the role of the methylammonium (MA) molecules in the Pb-I framework. Experiments indicate that the MA molecules are able to 'freely' spin around at room temperature even though they carry an intrinsic dipole moment. We have performed large supercell (2592 atoms) finite temperature *ab-initio* molecular dynamics calculations to study the correlation between the molecules in the framework. An underlying long range anti-ferroelectric ordering of the molecular dipoles is observed. The dynamical correlation between neighboring molecules shows a maximum around room temperature in the mid-temperature phase. In this phase, the rotations are slow enough to (partially) couple to neighbors via the Pb-I cage. This results in a collective motion of neighboring molecules in which the cage acts as the mediator. At lower and higher temperatures the motions are less correlated.

PACS numbers: 61.50.Ah, 65.40.-b, 88.40.-j

The spectacular rise of perovskite photovoltaics<sup>1</sup> has sparked much research effort into the physical mechanisms behind these materials' good photovoltaic performance. From a solid state physics perspective, the answer seems simple: the well suited electronic structure of methylammonium lead-iodide (MAPbI<sub>3</sub>). With a band gap of  $\sim 1.6$  eV<sup>2-6</sup> and a high absorption coefficient<sup>2,5,6</sup>, it is expected to be a high efficiency solar cell material for the solar radiation spectrum observed on earth.<sup>7</sup> Density Functional Theory (DFT) calculations have shown that an *s-p* mixture in the valence band maximum (VBM) and *p*-states in the conduction band minimum (CBM), combined with a direct band gap lead to an absorption coefficient up to an order of magnitude higher than GaAs.<sup>8</sup> However, the crystal structure of MAPbI<sub>3</sub> is completely different from GaAs. It even possesses temperature depended dynamical contributions arising from the organic constituent. The perovskite structure of MAPbI<sub>3</sub> is composed of three iodine atoms (monovalent anions) combined with a lead atom (divalent cation) and a CH<sub>3</sub>NH<sub>3</sub> (MA) molecule (monovalent cation). The Pb-I framework forms the perovskite structure out of PbI<sub>6</sub> octahedra and the molecules are trapped in the cavities. Whether the cubic perovskite structure is stable or becomes orthorhombic or tetragonal is determined by the temperature<sup>6</sup> combined with a balance between the size of the molecule and the Pb-I bond length.<sup>9</sup> NMR experiments have indicated that at high temperatures (>300 K) the MA molecule exhibits complete orientational disorder.<sup>10,11</sup> This means that the MA molecules have enough kinetic energy to overcome the rotational barriers and can rotate in their 'cage'. Around room temperature this process has a typical relaxation time of  $\sim 5$  ps.<sup>12</sup> These rotations apparently do not effect the charge carriers in the system, since very long electron-hole diffusion lengths have been reported.<sup>13,14</sup> From an

electronic point of view this is not surprising, because the Pb-I framework is electronically decoupled from the molecule.<sup>15</sup> The VBM/CBM are well separated from the HOMO/LUMO of the molecule, respectively. Therefore all conducting states for holes and electrons are dominated by the framework. At the same time the dispersion at the VBM and CBM is large, resulting in low effective masses.<sup>16</sup> However, this picture applies to 0 K and does not take into account the dynamics of the MA molecules, their order or lack thereof at room temperature (RT). A partial alignment of these polar molecules could result in polar domains. Piezoresponse force microscopy measurements seem to indicate that polar domains form and that spontaneous polarization occurs at RT.<sup>17,18</sup> A DFT based analysis indicates that at high temperature ferroelectricity is suppressed by the large configurational entropy and only below 50 K would ferroelectric (FE) ordering be present.<sup>19</sup> A strong argument against a polar structure is the absence of second harmonic generation in time-resolved pump-probe measurements.<sup>20</sup> The presence of polarized domains at RT is however still debated.

In a recent work we showed that polar phonons in MAPbI<sub>3</sub> increase the static dielectric constant to  $\sim 30$ , but they are too slow to effectively screen the excitonic state in the system.<sup>21</sup> The rotational dynamics of the polar MA molecules and the corresponding screening occurs at even lower frequencies.<sup>22-24</sup> Therefore even when the temperature is raised to RT, *i.e.* when the molecules rotate, the excitons are not screened by polar phonons nor by rotating polar molecules.<sup>21</sup> However, understanding of the dynamics of the molecules at finite temperatures is necessary to describe thermal transport<sup>25,26</sup> as well as the screening of free charge carriers.<sup>27</sup> The dynamics and (dis)order of the MA molecules in MAPbI<sub>3</sub> have been extensively investigated, both experimentally and theoretically. Experiments showed the ability of molecules

to reorient at RT with relaxation times in the range (1-10 ps).<sup>10,12,28-31</sup> The dynamics of the MA molecules in the PbI framework were also studied using *ab-initio* molecular dynamics reporting relaxation times in roughly the same picosecond time scale.<sup>32-37</sup> Most *ab-initio* studies were performed with small systems. A recent study of the relaxation time as a function of temperature using a reasonably large super cell indicates an absence of spatial correlation at RT.<sup>36</sup> However, a precise assessment of finite size effects in *ab-initio* calculations is still missing. MA dynamics in large supercells has been studied by classical molecular dynamics.<sup>38</sup> In agreement with experiment<sup>12</sup> a transition from the anti-ferroelectric ordering in the orthorhombic phase to thermally activated directional disorder in the tetragonal and cubic phases was reported.<sup>38</sup> However, the accuracy of model potentials is questionable and there is the need for an *ab-initio* validation. In particular, no systematic analysis of the spatial and dynamical correlation has been reported.

In this work we study the long range order of the MA molecules in MAPbI<sub>3</sub> by means of large scale *ab-initio* molecular dynamics (MD) calculations at finite temperatures. We show that the dynamics of the molecules is not a completely random thermal motion. Besides the possible dipole-dipole interaction between the intrinsic dipole moments of the molecules<sup>39</sup>, the order of the molecules is also mediated by long range cage stress and strain effects as well as deformations or rotations of the PbI<sub>6</sub> octahedra and their long range order. In the low temperature (<150 K) phase this leads to an anti-ferroelectric arrangement of the molecules.<sup>40-42</sup> At higher temperatures the ordering pattern changes.

The paper is organized as follows. In the next section, the details of the computational method are presented. Hereafter, we present the different super cell structures and their implications. We discuss in section III the dynamics of the molecules individually and in section IV the correlation with their neighbors. We discuss the results in V, and in the last section we summarize our findings in conclusions.

## I. COMPUTATIONAL METHOD

For the first-principles molecular dynamics calculations we use a plane-wave basis and the projector augmented wave (PAW) method<sup>43</sup> as implemented in the VASP code<sup>44-46</sup>. The PBEsol (Perdew, Burke, Ernzerhof modified for solids)<sup>47</sup> functional is used. Relatively shallow pseudo-potentials are used, for Pb the (6s<sup>2</sup>6p<sup>2</sup>), for I the (5s<sup>2</sup>5p<sup>5</sup>), for C the (2s<sup>2</sup>2p<sup>2</sup>) and for N the (2s<sup>2</sup>2p<sup>3</sup>) orbitals are included in the valence. This makes it possible to set a relatively low energy cut-off of 250 eV for the plane-wave basis.

Super cells of dimension  $n \times n \times n$ ,  $n = 2, 4, 6$  were constructed out of pseudo-cubic unit cells (12 atoms) with experimental lattice constants ( $a, b = 6.3115$  Å,  $c = 6.3161$  Å)<sup>6</sup> as described in Ref. 21. In order to

construct an unbiased starting structure, all molecules in the supercell are randomly (R) rotated over three axis before starting the MD run. In the supercell all atoms were allowed to move while keeping the lattice vectors fixed.

Gaussian smearing with  $\sigma = 0.05$  eV is used to broaden the one-electron levels. The Brillouin zone is sampled by the  $\Gamma$  point only for the large  $4 \times 4 \times 4$  (4-cell) and  $6 \times 6 \times 6$  (6-cell) supercells and by a  $(2 \times 2 \times 2)$   $\Gamma$ -centered Monkhorst-Pack grid for the  $2 \times 2 \times 2$  supercell (2-cell). Using only a single k-point for the 2-cell results in significant errors in the calculated forces. The Kohn-Sham orbitals are updated in the self-consistency cycle until an energy convergence of  $10^{-4}$  eV is obtained. A Langevin thermostat<sup>48</sup> is applied to simulate a canonical ensemble (at constant temperature). The trajectory is formed by propagating the structure with the calculated Hellmann-Feynman forces with time steps of 2.0/2.0/3.0 fs and increased hydrogen masses of 4/4/8 a.u. for the 2/4/6-cell, respectively. The hydrogen masses are increased to allow for a larger time step for the large cell-sizes. Additionally in the 6-cell the Pb and I masses have been decreased to 20 a.u. These changes in the masses are possible since the DFT functional does not depend on the mass and since the partition function factorizes into a momentum and position dependent part ( $\rho(X, P) = e^{-U(X)\beta} e^{-P^2/(2M)\beta}$ ) so that results for the configurational part  $X$  are independent of the chosen masses ( $M$ ). The down side is that the dynamical properties (velocities, average reorientation times, etc.) are no longer exact. However, differences in the dynamical properties between calculations where the same masses are used remain meaningful.

Unit cells for the different crystal phases have been constructed based on experimental crystal structures determined by X-ray diffraction. For the orthorhombic structure the Pb-I positions of Baïke *et al.*<sup>42</sup> were used ( $a = 8.8362$  Å,  $b = 8.5551$  Å,  $c = 12.5804$  Å) and for the tetragonal structure the Pb-I positions of Stoumpos *et al.*<sup>6</sup> were used ( $a = 8.8490$  Å,  $b = 8.8490$  Å,  $c = 12.6420$  Å). The molecules were placed in an arbitrary but unpolarized pattern and a high temperature MD (500 K, Pb-I framework kept fixed) was performed, allowing the molecules to reorient themselves. Several low energy structures were picked from the MD trajectory and for those all atoms were thoroughly relaxed (forces  $< 10^{-5}$  eV/Å) into their instantaneous ground state while keeping the lattice vectors fixed. The resulting lowest energy configurations are shown in Figure 1.

## II. MOLECULAR DYNAMICS: UNIT AND SUPERCELLS

In the MAPbI<sub>3</sub> structure the different MA molecules can interact with each other, either directly via the electrostatic forces (they are cations and have an intrinsic dipole moment) or indirectly by their collective pushing and pulling on the Pb-I framework. The potential energy

related to dipole-dipole interactions between the different molecules falls off like  $r^{-3}$ , and we expect that this interaction only influences the nearest neighbors. However, it is clear that a single unit cell, be it orthorhombic (4 formula units), tetragonal (4 formula units) or cubic (1 formula unit) is prone to finite size effects/self-interaction errors and might therefore be artificially stabilized in a particular ordering pattern. If these effects are ignored and one starts with the structures obtained by X-ray diffraction<sup>6,42</sup> for the three different phases, well ordered patterns are obtained as shown in Figure 1. These structures agree (at various levels of accuracy) with the orthorhombic<sup>49–51</sup> and tetragonal<sup>52,53</sup> molecular ordering patterns found in other first principles studies.

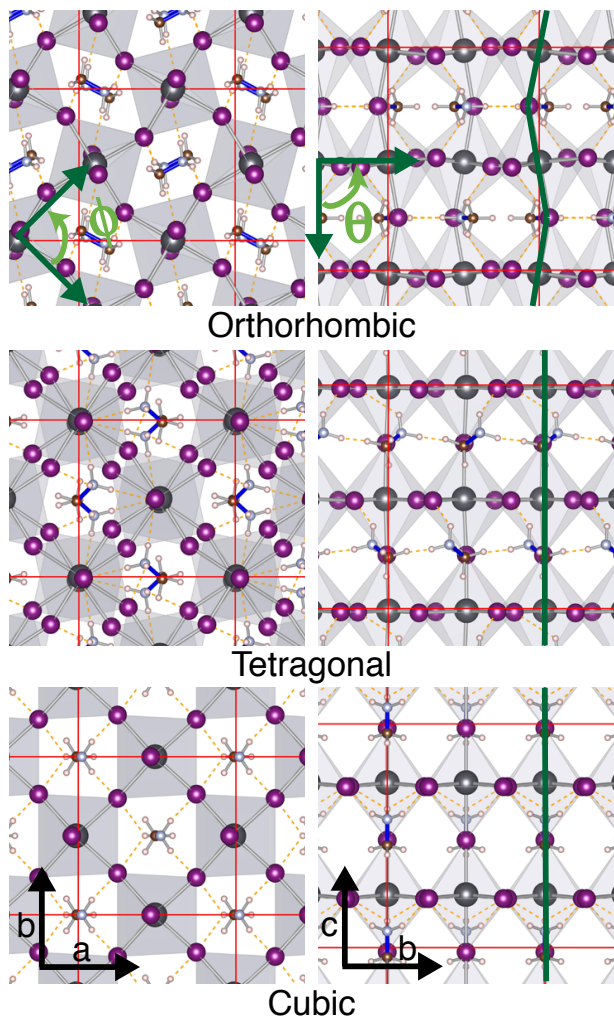


FIG. 1. (color online) The three different  $\text{MAPbI}_3$  crystal phases. The unit cells (48 atoms, 4 molecules, solid red lines) are indicated, except for the cubic phase where a  $\sqrt{2} \times \sqrt{2} \times 2$  supercell of the pseudo-cubic unit cell is shown. The dashed orange lines show the hydrogen bonds between the  $\text{NH}_3$  groups and the iodines. The left/right column shows a top/side view, respectively. The polar coordinates reference frame  $\{\phi, \theta\}$  to describe the orientation of the C-N bond of the MA molecule is drawn on the top.

The three crystal phases have distinct molecular ordering patterns:

The *orthorhombic phase* has an antiferroelectric (AFE) ordering pattern of the MA molecules, with two molecules lying flat in the  $ab$ -plane with a  $\sim 60^\circ$  angle between them. The layer on top has the same relative orientation in the plane, but the molecules are  $180^\circ$  degree rotated resulting in a zero net dipole moment. The  $\text{PbI}_6$  octahedra are rotated by  $\sim 15^\circ$  degree in the plane, one clockwise, and the other counterclockwise. The octahedra in the layer below have the same rotations in the  $ab$ -plane. An alternating  $\pm 11^\circ$  tilt from the  $c$ -axis of neighboring octahedra results in a zigzag pattern in the  $c$ -direction.

In the *tetragonal phase* the octahedra are aligned to the  $c$ -axis, but in the  $ab$ -plane the octahedra in the two layers do not have the same rotations. They are rotated by  $\sim 12^\circ$  degree, again one clockwise and the other counterclockwise. But in the second layer the order is reversed, i.e., counterclockwise and clockwise. In this Pb-I framework the MA molecules have an orthogonal orientation (when projected) in the  $ab$ -plane to all their nearest neighbors and have a  $\sim 30^\circ$  out of the  $ab$ -plane tilt. The resulting angle between all nearest neighboring molecules thereby becomes  $\sim 75^\circ$ . The total MA pattern here is slightly FE.

In the *cubic phase* the octahedra are almost not rotated and all molecules are aligned in a FE ordering pattern. At the corresponding temperature this state is dynamically unstable and the molecules are rotating.<sup>10,11</sup>

Overall, we see that the nitrogen (most electronegative) side of the molecules is close to the iodines. The average distance of the N atom to nearest neighbor (n.n.) I atoms is  $3.58 \pm 0.04 \text{ \AA} / 3.64 \pm 0.02 \text{ \AA}$  and of the C atom to n.n. I atoms is  $3.94 \pm 0.02 \text{ \AA} / 4.02 \pm 0.09 \text{ \AA}$ , for the orthorhombic/tetragonal structure, respectively. The N-H bonds align to the N-I directions, thereby forming hydrogen bonds.<sup>54,55</sup> All H-I bonds with a length  $\leq 3 \text{ \AA}$  have been indicated in Fig. 1 by the dashed (orange) lines. This orientation reduces the electrostatic energy between the negatively charged iodines and positively charged molecule. It dominates over the intermolecular dipole-dipole interaction as can be seen in the tetragonal structure (with its rotated octahedra), where it stabilizes the FE pattern.

Now we move on to supercells and see if and how these ordering patterns prevail at finite temperature. Previous ab-initio MD calculations have used relatively small supercell structures of 8 formula units (cubic)<sup>33,56</sup> or 32 formula units (tetragonal)<sup>34,56,57</sup>. Only Carignano *et al.*<sup>34</sup> have systematically studied the effect of the supercell size and performed a calculation on a 108 formula unit (tetragonal) super cell. Using classical molecular dynamics Mattoni *et al.* have studied a 256 formula unit (orthorhombic) supercell.<sup>38</sup> An overview of the supercells that we have evaluated at room temperature and below is presented in Table I. We have constructed  $n \times n \times n$  supercells of the pseudo-cubic structure (1 formula unit),



TABLE I. Overview of structures evaluated by molecular dynamics. Super cells of  $n \times n \times n$  cubic unit cells, starting with an unpolarized-random (R) or polarized-aligned (A) MA ordering pattern, have been propagated for T picoseconds in steps of dt femtoseconds, with hydrogen mass  $M_H$  and at different temperatures.

Size	T (ps)	dt (fs)	$M_H$ (a.u.)	Temp (K)
$2 \times 2 \times 2$ (R1)	86	2.0	4	300
$2 \times 2 \times 2$ (R2)	63	2.0	4	300
$2 \times 2 \times 2$ (R3)	64	2.0	4	300
$2 \times 2 \times 2$ (A)	84	2.0	4	300
$4 \times 4 \times 4$ (R)	21	2.0	4	100
$4 \times 4 \times 4$ (R)	27	2.0	4	150
$4 \times 4 \times 4$ (R)	42	2.0	4	200
$4 \times 4 \times 4$ (R)	24	2.0	4	250
$4 \times 4 \times 4$ (R)	23	2.0	4	300
$4 \times 4 \times 4$ (A)	31	2.0	4	300
$4 \times 4 \times 4$ (R)	31	2.0	4	400
$6 \times 6 \times 6$ (R)	8	3.0	8	150
$6 \times 6 \times 6$ (R)	13	3.0	8	300

thereby containing  $N = n^3$  molecules. This is hereafter referred to as the  $n$ -cell. The lattice parameters of the pseudo-cubic structure are fixed at the experimental values, while all internal coordinates have been fully relaxed at the DFT level. During the MD all atoms are allowed to move, but the cell volume and shape are kept fixed. Since we are evaluating large cells this approximation seems acceptable and the error diminishes going from  $n = 2$  to  $n = 6$ . From the trajectory of all atoms we extract the orientation of all MA molecules (C-N bond vector) in polar coordinates projected on the unit sphere ( $\phi_i(t), \theta_i(t)$ ). The coordinate frame is aligned to the Pb-I framework, as shown in Fig. 1. Initially, all molecules in the super cells were randomly rotated over three axes to generate an unbiased starting structure. We have tested this in comparison to a starting structure with aligned molecules and found that this approach results in shorter equilibration times. For example, the first 20 ps of an MD trajectory at 300 K for an initially aligned 4-cell involve a reorientation of the molecules so that the initial long range order is practically destroyed. Starting from a random state avoids these long equilibration times. This can be seen in Figure 2, where the average polarization based on the molecular contribution only,

$$P_{\text{mol}}(t) = \left| \frac{1}{N} \sum_{i=1}^N \hat{\mathbf{p}}_i(t) \right|, \quad (1)$$

has been plotted for a polarized-aligned (A) and a unpolarized-random (R) starting structure. This is not the full polarization of the structure, which would include contributions from the cage, but merely the contribution of the intrinsic dipole moment vector ( $\hat{\mathbf{p}}_i$ ) of each molecule. Here we assume that the dipole of each molecule is equally strong and that it does not change in time. After initial equilibration time, both calculations show a fluctuating behavior around a mean value.

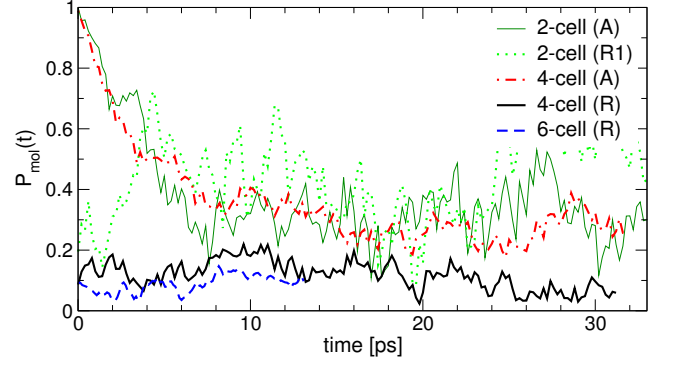


FIG. 2. (color online) Molecular polarization  $P_{\text{mol}}(t)$  in the 2-cell, 4-cell, and 6-cell at 300 K starting from an unpolarized-random (R) structure. The polarization resulting from a polarized-aligned (A) starting structure in the 4-cell is given for comparison.

The mean value depends on the starting configuration and does not converge to a common value within the available compute time. The higher degree of fluctuation might indicate that the (A) system is not yet as well equilibrated as the (R) system.

### III. DYNAMICS OF INDIVIDUAL MOLECULES

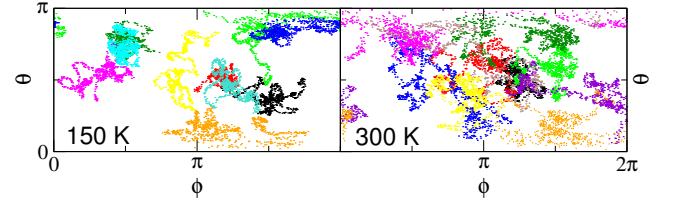


FIG. 3. (color online) The polar plot of 10 randomly chosen dipoles in the 6-cell shows the rotational mobility ( $\phi_i(t), \theta_i(t)$ ) in a time frame of 8 ps at 150 K and 300 K.

We now want to determine how rotationally mobile the individual molecules are. In Figure 3 the coordinates ( $\phi_i(t), \theta_i(t)$ ) of 10 randomly chosen molecules in the 6-cell have been plotted over a time frame of 8 ps. The area covered by the paths increases with temperature. At 150 K the average orientation of most of the dipoles is maintained. At 300 K the covered area of the path ways is so large that reorientation of the molecules by  $180^\circ$  is possible. How exactly the molecules move at 300 K is not yet clear, i.e., whether they perform free rotations or jump from one preferential orientation to the next, as was recently suggested.<sup>31</sup>

The average reorientation time ( $\tau_{\text{mol}}$ ) of the  $N$  molecules can be extracted from the autocorrelation function

$$r_{\text{mol}}(t - t_0) = \frac{1}{N} \sum_{i=1}^N \hat{\mathbf{p}}_i(t_0) \cdot \hat{\mathbf{p}}_i(t), \quad (2)$$

where the dot product traces the change of the molecule's orientation in time with respect to its orientation at  $t = t_0$ . The autocorrelation function is smoothed by applying a time averaging over  $N_T$  different starting times  $t_0$ ,

$$\langle r_{\text{mol}}(t) \rangle = \frac{1}{N_T N} \sum_{j=0}^{N_T-1} \sum_{i=1}^N \hat{\mathbf{p}}_i(\Delta t j) \cdot \hat{\mathbf{p}}_i(t + \Delta t j), \quad (3)$$

where  $\Delta t = \frac{T}{2(N_T-1)}$  for  $N_T > 1$ . Within this definition  $\langle r_{\text{mol}}(t) \rangle$  is computable only for half of the total MD trajectory time  $T$ . In Figure 4 a), the autocorrelation functions of MA molecules in the 2,4, and 6-cell structure at 300 K are shown.  $\tau_{\text{mol}}$  is the time at which the autocorrelation function reaches the value  $1/e$ . Even though the autocorrelation functions are averaged with Eq. 3 and long MD trajectories were used, the relaxation times are different and depend on the starting configuration. In the 2-cell, using the aligned (A) molecules as a starting structure results in faster dynamics than randomly (R) oriented molecules. However, even between different random structures, R1, R2 and R3 the  $\tau_{\text{mol}}$  values differ. Some starting configurations are energetically more disfavored and might therefore be easier to break down. This means that with the present results for the 2-cell, we have an uncertainty in the  $\tau_{\text{mol}}$  value of about  $\pm 3$  ps. To reduce the uncertainty, one has to improve the statistics. This can be done by averaging over many more MD trajectories using different random starting configurations.

The values  $\tau_{\text{mol}}$  for the different systems have been tabulated in Table II. They have been obtained by fitting an exponentially decaying function to the curves. These calculations show that  $\tau_{\text{mol}}$  in the 4-cell is at least of the same order as in the 2-cell, however with the present data we cannot conclude with certainty that the reorientation time is not affected by finite size effects. Note that the  $\tau_{\text{mol}}$  values are overestimated because the hydrogen masses have been raised. This raises the molecule's moment of inertia, while the DFT forces remain unchanged. The 6-cell shows a slightly lower reorientation time, which is possibly an artifact from the lower Pb and I masses (see Computational Details Section).

Figure 4 b) shows the autocorrelation function in the 4-cell for various temperatures. The corresponding  $\tau_{\text{mol}}$  values are 3.5, 6.9, 9.9, 18, 32 and 69 ps for 400, 300, 250, 200, 150 and 100 K, respectively. For temperatures below 200 K these numbers do not have a significant meaning. At these temperatures the autocorrelation function is not well described by a simple exponential.<sup>38</sup> Analysis with

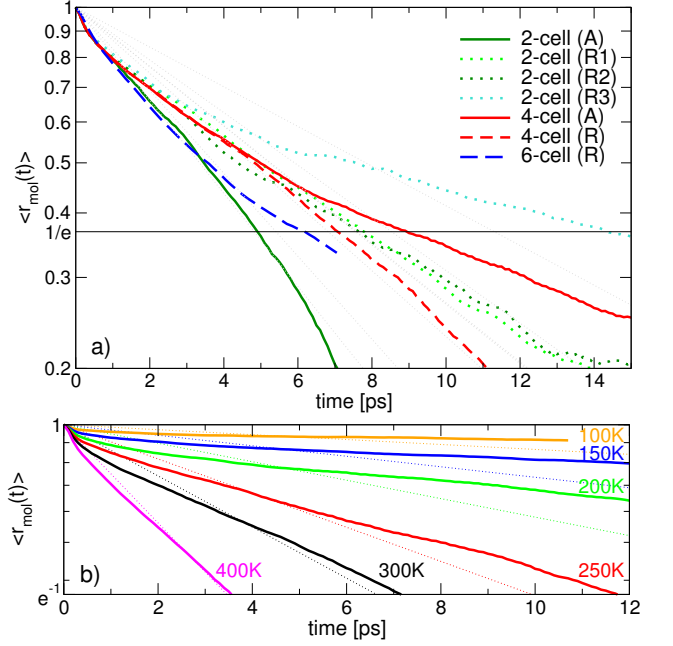


FIG. 4. (color online) Autocorrelation function  $\langle r_{\text{mol}}(t) \rangle$  of MA molecules in semi-log plot. a) At 300 K in the 2,4, and 6-cell structures starting from random (R) and aligned (A) configuration of the molecules. b) At various temperatures in between 100-400 K in the 4-cell. The dashed lines indicate exponential fits.

jump models on temperature dependent neutron scattering data shows relaxation time values of the same order.<sup>12</sup> Compared to this experiment here the presented results in the mid-temperature phase (150-300 K) are slightly lower.

In order to understand the molecular order at 300 K, the polar distribution of the orientation ( $\phi_i(t), \theta_i(t)$ ) of all molecules in the cell over the entire simulation time ( $T$ ) is plotted in Figure 5. The distribution is plotted for the 2, 4 and 6-cell. Provided that a sufficiently long simulation time is taken at 300 K, the polar distributions are independent of the precise starting configuration. Here, MD trajectories from different starting molecular orderings (A/R) were combined in a single polar plot. The polar distributions of trajectories starting from the aligned and the three random structures for the 2-cell have been combined (A+3R). For the 4-cell, the full trajectory starting from the random configuration and the second half of the trajectory of the aligned starting configuration have been combined (A+R). This removes the strong artificial bias of aligned ordering. The differences in the distribution between the 2-cell and the larger 4,6-cells are small. The remaining differences are predominantly related to the insufficient statistics. This means that the effective potential in which the molecules move does not depend strongly on cell size. (The effective potential can be obtained by a Boltzmann inversion of the polar distribution.) Combined with the foregoing observation of similar  $\tau_{\text{mol}}$  times this indicates that

TABLE II. The relaxation time ( $\tau_{\text{mol}}$ ) in picoseconds for a  $n$ -cell at 300 K starting from a polarized-aligned (A) and unpolarized-random (R) structures.

$n$	2 (A)	2 (R1)	2 (R2)	2 (R3)	4 (A)	4 (R)	6 (R)
$\tau_{\text{mol}}$	4.8	7.6	7.6	11.3	8.5	6.8	5.4

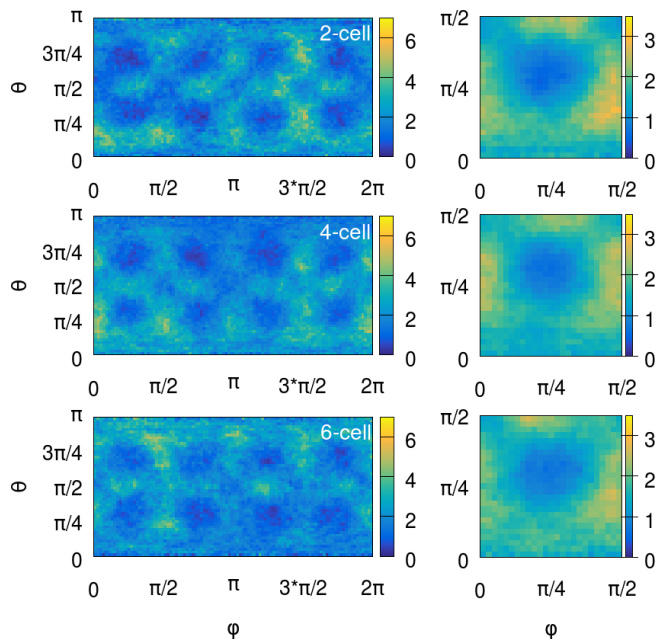


FIG. 5. (color online) Polar angle distribution of the MA molecules at 300 K in the 2-cell (top), 4-cell (middle) and 6-cell (bottom). The plots show the full rotational space (left) and the down-folded plot (right) into  $1/8$  of the full space.

the dynamics of the individual molecules are roughly the same in the 2-, 4- and 6-cell. The polar plots presented in Fig. 5 are in agreement with the 300 K ab-initio/classical MD calculations in Refs. 34/38, respectively. The regular pattern in the polar plots shows the presence of cubic symmetry. Therefore we have down-folded the polar plots into a single octant, shown on the right. The hole in the middle of the down-folded plot corresponds to the room-diagonal orientation of the Pb-I cube. This orientation is systematically avoided by the MA molecules. Instead, the preferred direction is close to the face diagonal. The plot also shows that almost all orientations except the room-diagonal orientation have a fairly high probability. These results agree with the picture arising from NMR measurements. At room temperature the molecules are rotating freely in a potential with several preferred high symmetry directions.<sup>11</sup>

When the temperature of the system is lowered, a more anisotropic polar angle distribution appears. In Figure 6 the down-folded polar plots of a 4-cell at temperatures between 400 and 100 K are shown. When cooling down, the pattern changes from a ring with three spots, to just two spots below 200 K. We are not able to pin-down the phase transition temperature to the orthorhombic/low-temperature phase (exp.  $\sim 150$  K<sup>6</sup>) exactly. Figure 6 indicates that the low-temperature phase in our supercell approach is related to the freezing in of the molecules into two preferred orientations in the down-folded polar plot. The high temperature patterns show a similar polar distribution as the ones calculated by the classical MD calculations of Mattoni *et al.* in Ref. 38. How-

ever, for temperatures below 250 K there are some differences. The most prominent difference appears at 100 K, where we find two distinct spots in the down-folded polar plot instead of one. The first and most dominant spot is close to  $(\phi = \pi/3, \theta = \pi/2)$ , a direction where the molecules are in the  $xy$ -plane and are slightly tilted off the face diagonals of the Pb-I framework. The second spot close to  $(\phi = 0, \theta = \pi/6)$  is absent in Ref. 38. What has happened is more easy to identify in the full polar plot, as shown in Figure 7 (top). As mentioned before in the orthorhombic structure (Fig. 1) all molecules lie flat in the  $xy$ -plane with a  $\sim 60^\circ$  angle to their neighbors and an AFE stacking in the  $z$ -direction. These four distinct orientations are presented by the black circles in the symmetrical polar plot of Fig. 7 (bottom). The second spot also describes such a pattern, but with the molecules in the  $xz$ -plane (presented by the red squares). This shows that, while cooling down the system, we acquired two competing orthorhombic phases ( $xy$  and  $xz$ , circles and squares in Fig. 7) in the supercell. This low-temperature phase does not represent the ground state minimum, but as a result of the rapid cooling rate the system has been trapped in a local minimum. To avoid confusion we refer to this mixed phase in the supercell as the low-temperature phase. We furthermore note that the condensation into ordered phases with molecules lying in the  $xy$  or  $xz$  plane occurred even though we used the pseudo-cubic initial structure.

The general picture that appears in Fig. 6 about the transition of the molecular order in the supercell from the low-temperature (100 K) to the high-temperature (300 K) phase is one of three competing orthorhombic phases, with molecules in the  $xy$ ,  $xz$  and  $yz$  planes. When the temperature increases, more than one phase can be present and the ideal spots start to blur out. This process goes on until a closed ring is formed for temperatures  $> 300$  K. Within the available simulation time, we have not observed a 'pure' tetragonal phase in the mid-temperature regime. According to the unit cell of Fig. 1 the tetragonal phase should result in four spots at  $\{\phi = n \cdot \pi/2, \theta = \pi/3\}$  with  $n = 0, 1, 2, 3$ . Therefore our mid-temperature phase is most likely to be a mixture between the orthorhombic phases rather than a representative of the tetragonal structure. We return to this point in Fig. 9.

At this point we have presented the orientation of the set of all molecules and their average reorientation times, but we do not know about the order between neighboring molecules. To this end, one needs to study the correlation between molecules.

#### IV. CORRELATION BETWEEN MOLECULES

In the previous two sections we have described the behavior by averaging over all molecules (Sec. II) and the behavior of each molecule individually (Sec. III). In this section the correlation between the orientation of

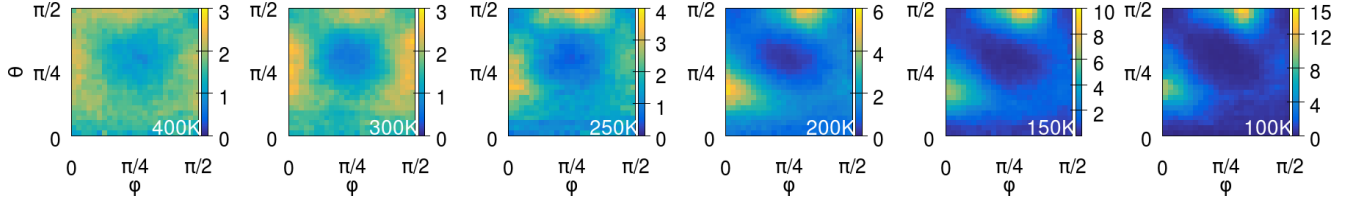


FIG. 6. (color online) From left to right, down-folded polar angle distribution of the MA molecules at 400, 300, 250, 200, 150, 100 K in the 4-cell.

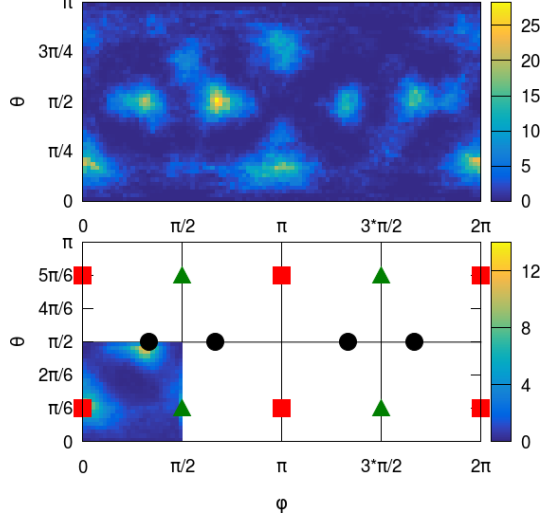


FIG. 7. (color online) *Top*: Polar angle distribution of the MA molecules at 100 K in the 4-cell. *Bottom*: Ideal molecular ordering of the orthorhombic structure with the molecules in the  $xy$ -plane (black circles), the  $xz$ -plane (red squares) and in the  $yz$ -plane (green triangles) with a  $\pi/3$  relative orientation. The down-folded polar angle distribution is included for comparison.

a molecule and its nearest neighbors (n.n.) is studied both in time (*dynamical correlation*) and on time average (*static correlation*).

### A. Static correlation

The dot product between the unitary dipole vectors of molecules  $i$  and  $j$

$$d_{i,j}(t) = \hat{\mathbf{p}}_i(t) \cdot \hat{\mathbf{p}}_j(t), \quad (4)$$

indicates whether the molecules are arranged to be parallel (1), orthogonal (0) or anti-parallel ( $-1$ ). All other relative orientations are within the range  $([-1, 1])$ . We focus on the orientation of one molecule with respect to molecules at different distances/directions:  $|\mathbf{q}| = |(k, l, m)|$ . Here  $k, l, m$  are integers ( $1, \dots, n$  for an  $n$ -cell) describing the connecting vector between molecules  $i$  and  $j$  on a cubic grid. Figure 8 shows the time averaged distribution of  $d_{i,j}$  over the whole trajectory of the MD simulation for the 2-, 4-, and 6-cell at 300 K. The first

observation is that all relative orientations occur in all simulated  $n$ -cells. Second, the shape of the distribution, characterized by the positions of the maxima and minima, does not depend very significantly on the cell size. Uncorrelated dipoles would result in a flat distribution, and therefore some correlation prevails at 300 K. The differences between the 2-, 4- and 6-cell are related to the limited simulation time for the large supercells. Initially the molecules have a random orientation, and therefore it takes simulation time to bring the flat distribution to the converged attenuated distribution. For the computationally less expensive 2-cell calculations these results are very close to the fully converged distribution for  $|\mathbf{q}| = 1$  and  $\sqrt{2}$ . Note that a combined trajectory of  $\sim 300$  ps corresponding to four MD runs starting from different molecular ordering (A+3R) was necessary.

In the 1st n.n. shell ( $|\mathbf{q}| = \sqrt{1}$ ) of Fig. 8, one 'sharp' peak at  $d_{i,j} = -1$  is observed, here the molecules are AFE aligned. A second broad peak is found at  $d_{i,j} = 0.4$ , indicating a  $\sim 66^\circ$  angle between the neighboring dipoles. Going to the 2nd n.n. shell ( $|\mathbf{q}| = \sqrt{2}$ ), a similar pattern is observed, but mirrored. The sharp peak at  $d_{i,j} = 1$  indicates a FE alignment between a molecule and its 2nd n.n. The broad peak is also observed, but is now at  $d_{i,j} = -0.4$  indicating a  $\sim 114^\circ$  angle. For the 4- and 6-cells, the third distribution ( $|\mathbf{q}| = \sqrt{3}$ ) is almost exactly the same as the first. When going even further to the 4th ( $|\mathbf{q}| = \sqrt{4}$ ) and 7th ( $|\mathbf{q}| = \sqrt{8}$ ) shells the same pattern prevails. This alternating or 'mirror' pattern is not an effect of the supercell size, since it does not diminish going from the 4- to the 6-cell.

The distributions in Figs. 8 a-c) show an average over the different directions, all neighbors at the same distance have been added. This is possible because there is almost no cubic symmetry breaking, as can be seen in Figs. 8 d-e). The static correlation along the cubic axis ( $\mathbf{q}_x, \mathbf{q}_y$  and  $\mathbf{q}_z$ ) is shown in Fig. 8 d) and for all face-diagonal neighbors ( $\mathbf{q}_{xy}, \mathbf{q}_{yz}$  and  $\mathbf{q}_{xz}$  separately) in Fig. 8 e). The curves have the same shapes and maxima, but the relative intensity per peak varies slightly.

Analysis of Fig. 8 confirms the picture deduced from the polar angle plots, i.e., that the molecular ordering pattern at 300 K is a mixture of orthorhombic phases smeared out by the high temperature. Plots of the distribution in the 4-cell at different temperatures further justify this view. The distributions for the 1st and 2nd n.n. shell are shown in Figure 9. For comparison the



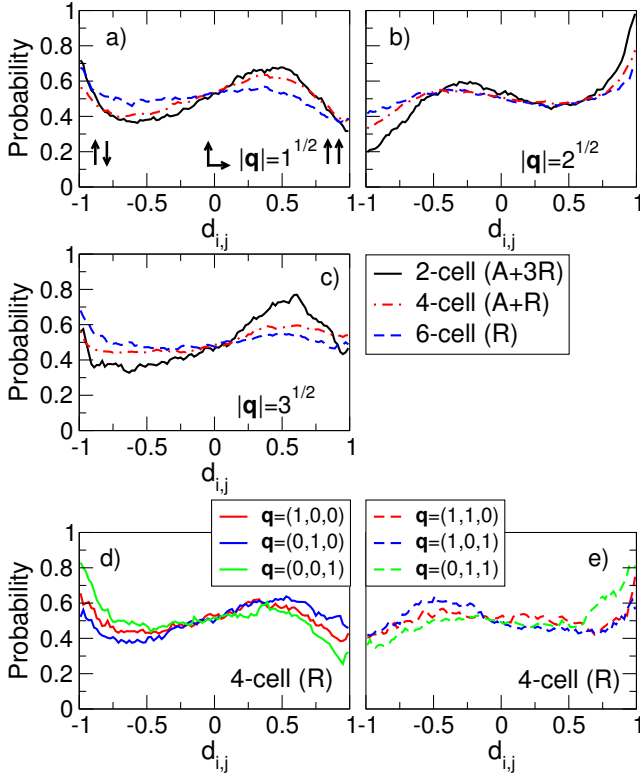


FIG. 8. (color online) Static correlation between molecules at 300 K in the a) 1st, b) 2nd and c) 3rd n.n. shells expressed by the distribution of  $d_{i,j}$ , going from AFE ( $\uparrow\downarrow$ ) to FE ( $\uparrow\uparrow$ ) alignment. The red/blue/green lines correspond to the 2-cell/4-cell/6-cell, respectively. The three different directions for the d) 1st (cubic axis) and the e) 2nd (face-diagonal) n.n. in the 4-cell at 300 K. (Integral of the  $d_{i,j}$  distributions are normalised to one.)

distribution in the perfect orthorhombic and tetragonal cells of Fig. 1 has been plotted by the solid (black) and dashed (red) histograms, respectively. When the system is cooled down the sharp AFE and broad  $\sim 60^\circ$  orientation peaks grow in relative intensity. These two peaks correspond to the molecular ordering pattern in the orthorhombic phase and are the same for the  $xy$ ,  $yz$  and  $xz$ -orientations. However, stress between the different phases in the supercell and the finite temperature can explain the shift and broadening of the peaks. The ratio between the most and least likely orientation is simultaneously increased from a factor of 2 at 300 K to a factor of 25 at 100 K, indicating the freezing in of a fixed ordered pattern going hand in hand with an increase of static correlation. Again, no clear signature of the tetragonal phase is found in the 4-cell.

### B. Dynamical correlation

As a measure of dynamical correlation between the MA molecules, we have calculated the Pearson correlation co-

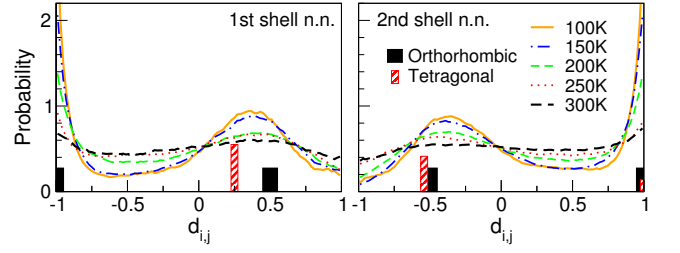


FIG. 9. (color online) Static correlation between molecules in the 1st (left) and 2nd (right) n.n. shell of the 4-cell at temperatures between 100 and 300 K expressed by the distribution of  $d_{i,j}$ . The dot product values corresponding to the ideal molecular ordering pattern in the orthorhombic/tetragonal phase are shown (in arb. units) by the filled/striped histograms, respectively.

efficient of the  $\theta_i(t)$  trajectories of neighboring molecules. Here we use the square Pearson correlation coefficient

$$r_{i,j}^2 = \left( \frac{\sum_{t=t_0}^T (\theta_i(t) - \bar{\theta}_i)(\theta_j(t) - \bar{\theta}_j)}{\sigma_i^2 \sigma_j^2} \right)^2, \quad (5)$$

with  $\sigma^2$  the variance and  $\bar{\theta}$  the mean of  $\theta(t)$ . It is an estimate of the fraction of the two signals showing linear correlation. In Figure 10 the average values  $r_c^2$  are plotted. This is the average  $r_{i,j}^2$  over all pairs  $i, j$  with distance  $d = |\mathbf{r}_i - \mathbf{r}_j|$  and ranges between 0-100%. 12 ps long trajectories of the 4-cell MD calculations at different temperatures have been used. Qualitatively the same picture appears when the dynamical correlation of  $\phi_i(t)$  with  $\phi_j(t)$  (dashed lines) or  $\phi_i(t)$  with  $\theta_j(t)$  (dotted lines) are calculated. Random dipoles placed on the 4-cell grid result in a mere  $\sim 0.02\%$  correlation. Remarkably, the dynamical correlation is temperature dependent and, even more remarkably, is independent of the distance, at least in the 4-cell considered here. This means that the movement of the molecules in the mid-temperature range is partly a collective motion. A recent Monte Carlo simulation based on a simplified model Hamiltonian of interacting MA molecules in MAPbBr<sub>3</sub> suggested correlation in clusters of 3 neighboring molecules.<sup>58</sup> We cannot predict an effective rotation cluster size (because of the limited supercell size), but in the 4-cell it seems to be greater than 3. The filled symbols in Fig. 10 correspond to the  $\theta_i\theta_j$  correlation in the 6-cell. At 300 K the same level of dynamic correlation as in the 4-cell is found, but at 150 K the value is larger. Presumably this is caused by the very limited simulation time and therefore too short equilibration time.

## V. DISCUSSION

In this next to last section, we would like to hypothesize about the origins of the dynamics of the MA molecules. J. Li *et.al.* already referred to it in Ref. 59



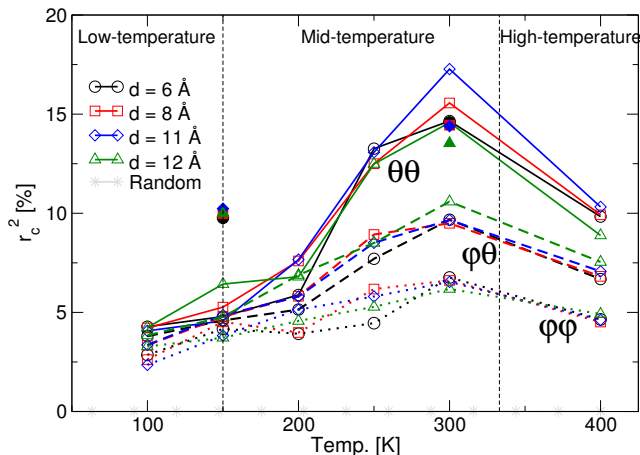


FIG. 10. (color online) Dynamical correlation between molecules in the first four n.n. shells of the 4-cell at temperatures between 100 and 300K expressed by square Pearson correlation coefficient ( $r_c^2$ ) for  $\theta_i\theta_j$ ,  $\phi_i\theta_j$  and  $\phi_i\phi_j$ . The filled symbols correspond to the  $\theta_i\theta_j$  correlation in the 6-cell. Experimental phase transition temperatures have been indicated by the dashed lines.

as the 'chicken and egg paradox' present in this system. Do the molecules determine the rotations of the  $\text{PbI}_6$  octahedra or do the molecules follow the octahedra? Their conclusion was that the two mechanisms work synergetically. The results presented here shed new light on this issue from a time and temperature dependent viewpoint. We focus now on the, at first sight, peculiar temperature dependence of the dynamical correlation in Fig. 10. A peak in the dynamical correlation at finite temperature is unusual. In most cases dynamical correlation decreases when temperature goes up. For example, the correlation between two next nearest neighboring atoms in a cubic crystal performing the (very correlated) motion associated to a phonon mode. If the temperature increases, modes tend to broaden and higher lying modes become occupied. This will lower the dynamical correlation between the atoms. However in Fig. 10, in the low-temperature phase, the molecules do not possess enough kinetic energy to overcome the potential barrier imposed by the Pb-I framework. Therefore at low temperatures, where the molecules only oscillate (random thermal motion) around their equilibrium positions and rotate along the C-N axis, the motion between neighboring molecules is less correlated. In the intermediate temperature phase the reorientation times ( $\tau_{\text{mol}}$ ) become finite. The molecules then have enough kinetic energy to overcome the potential barrier. However, because neighboring octahedra are rotated with respect to each other in the low and mid-temperature range, the potential landscape in these phases is expected to be less isotropic compared to the high-temperature (pseudo-cubic) phase. It is therefore likely that a molecule in the mid-temperature regime can only rotate if (some of) its surrounding molecules rotate as well. The collec-

tive reorientation prevents large stress and strain interactions with the Pb-I framework. When the temperature is raised (but remaining in the mid-temperature regime) more (concerted) reorientation pathways become available and the average level of dynamical correlation increases. When the temperature is raised even further into the high-temperature phase, the kinetic energy lies above the barriers imposed by the now more isotropic potential landscape of the cage and the molecules rotate independently. Overall, we suggest that the Pb-I framework is the mediator here, coupling molecule  $i$  with  $j$  and not the electrostatic dipole-dipole interaction, which would be distance dependent.

## VI. CONCLUSION

Large supercell ab-initio molecular dynamics calculations of the perovskite solar cell material  $\text{MAPbI}_3$  have been performed. The dynamics of the initially randomly oriented MA molecules has been studied and carefully analyzed with respect to the supercell size. We find that at 300 K the  $2 \times 2 \times 2$  (2-cell, 96 atoms),  $4 \times 4 \times 4$  supercell (4-cell, 768 atoms) as well as the  $6 \times 6 \times 6$  (6-cell, 2592 atoms) supercells result in very similar polar angle distributions of the molecules if the molecular dynamics trajectories are long enough. However, a small supercell (2-cell) can artificially constrain the dynamics of the molecules, it is more sensitive to the initial random orientations of the molecules. Therefore either long ( $> 100$  ps) trajectories have to be calculated or a combination of multiple shorter runs starting from different independent random starting configurations has to be made. The average reorientation times ( $\tau_{\text{mol}}$ ) in the three supercells are of the same order. The molecules can rotate with a  $\tau_{\text{mol}}$  time of  $\sim 7$  ps. This is an upper bound because increased hydrogen masses have been used. The molecules systematically avoid the room-diagonal orientation and prefer the (slightly tilted off) face-diagonal orientations of the 'cubical' Pb-I cage.

At room temperature all relative orientations between neighboring molecules can occur. However, signs of an ordering pattern related to the orthorhombic structure smeared out by the high temperature are visible. When the temperature is lowered to 100 K the molecular ordering pattern condenses into a mixture of orthorhombic phases within the supercell. The dynamical correlation, expressed by the Pearson correlation coefficient between the  $\theta(t)$  trajectories of neighboring molecules in the 4-cell, shows, in the considered temperature range of 100-400 K, a value between 5-15%. A purely random system of the same size would result in a mere 0.02% correlation. At room temperature a maximum in the dynamical correlation is observed. In this mid-temperature phase, the molecules possess enough thermal energy to rotate and this process is slow enough to couple to neighbors via the Pb-I cage. The range of the coupling extends throughout the entire considered supercell. This results in (par-

tially) collective motion of neighboring molecules driven by stress and strain interactions which are mediated by the Pb-I framework. The role of intermolecular dipole-dipole interactions is most likely negligible in this process. At lower temperatures, the motions are less correlated, because the molecules randomly oscillate around their fixed orientations. Also at higher temperatures there is less correlation, because the molecules spin around freely.

## ACKNOWLEDGMENTS

MB, CF, AK and DDS acknowledge funding by the joint project of the Indian Department of Science and Technology (DST) and the Austrian Science Fund (FWF): I1490-N19 (INDOX). GK and CF acknowledge funding by Austrian Science Fund (FWF): F4102-N28, F4115-N28 (SFB ViCoM). The calculations were performed at the Vienna Scientific Cluster (VSC-3). VESTA<sup>60</sup> was used for Fig. 1.

- 
- \* [menno.bokdam@univie.ac.at](mailto:menno.bokdam@univie.ac.at)
- <sup>1</sup> NCPV, “research cell efficiency records,” (2016).
  - <sup>2</sup> M. Hirasawa, T. Ishihara, and T. Goto, *J. Phys. Soc. Jpn.* **63**, 3870 (1994).
  - <sup>3</sup> K. Tanaka, T. Takahashi, T. Ban, T. Kondo, K. Uchida, and N. Miura, *Sol. State Comm.* **127**, 619 (2003).
  - <sup>4</sup> G. Papavassiliou and I. Koutselas, *Synthetic Metals* **71**, 1713 (1995).
  - <sup>5</sup> M. M. Lee, J. Teuscher, T. Miyasaka, T. N. Murakami, and H. J. Snaith, *Science* **338**, 643 (2012).
  - <sup>6</sup> C. C. Stoumpos, C. D. Malliakas, and M. G. Kanatzidis, *Inorg. Chem.* **52**, 9019 (2013).
  - <sup>7</sup> W. Shockley and H. J. Queisser, *J. Appl. Phys.* **32**, 510 (1961).
  - <sup>8</sup> W.-J. Yin, T. Shi, and Y. Yan, *Adv. Mat.* **26**, 4653 (2014).
  - <sup>9</sup> C. Li, X. Lu, W. Ding, L. Feng, Y. Gao, and Z. Guo, *Acta. Cryst. Sec. B* **64**, 702 (2008).
  - <sup>10</sup> R. Wasylishen, O. Knop, and J. Macdonald, *Sol. State Comm.* **56**, 581 (1985).
  - <sup>11</sup> T. Baikie, N. S. Barrow, Y. Fang, P. J. Keenan, P. R. Slater, R. O. Piltz, M. Gutmann, S. G. Mhaisalkar, and T. J. White, *J. Mater. Chem. A* **3**, 9298 (2015).
  - <sup>12</sup> T. Chen, B. J. Foley, B. Ipek, M. Tyagi, J. R. D. Copley, C. M. Brown, J. J. Choi, and S.-H. Lee, *Phys. Chem. Chem. Phys.* **17**, 31278 (2015).
  - <sup>13</sup> G. Xing, N. Mathews, S. Sun, S. S. Lim, Y. M. Lam, M. Grätzel, S. Mhaisalkar, and T. C. Sum, *Science* **342**, 344 (2013).
  - <sup>14</sup> S. D. Stranks, G. E. Eperon, G. Grancini, C. Menelaou, M. J. P. Alcocer, T. Leijtens, L. M. Herz, A. Petrozza, and H. J. Snaith, *Science* **342**, 341 (2013).
  - <sup>15</sup> A. Filippetti and A. Mattoni, *Phys. Rev. B* **89**, 125203 (2014).
  - <sup>16</sup> P. Umari, E. Mosconi, and F. D. Angelis, *Sci. Rep.* **4**, 4467 (2014).
  - <sup>17</sup> Y. Kutes, L. Ye, Y. Zhou, S. Pang, B. D. Huey, and N. P. Padture, *J. Phys. Chem. Lett.* **5**, 3335 (2014).
  - <sup>18</sup> H.-S. Kim, S. K. Kim, B. J. Kim, K.-S. Shin, M. K. Gupta, H. S. Jung, S.-W. Kim, and N.-G. Park, *J. Phys. Chem. Lett.* **6**, 1729 (2015).
  - <sup>19</sup> A. Filippetti, P. Delugas, M. I. Saba, and A. Mattoni, *J. Phys. Chem. Lett.* **6**, 4909 (2015).
  - <sup>20</sup> S. G. P. Mahale, B. P. Kore, S. Mukherjee, M. S. Pavan, C. De, S. Ghara, A. Sundaresan, A. Pandey, T. N. G. Row, and D. D. Sarma, *J. Phys. Chem. Lett.* **7**, 2412 (2016).
  - <sup>21</sup> M. Bokdam, T. Sander, A. Stroppa, S. Picozzi, D. D. Sarma, C. Franchini, and G. Kresse, *Sci. Rep.* **6**, 28618 (2016).
  - <sup>22</sup> M. A. Pérez-Osorio, R. L. Milot, M. R. Filip, J. B. Patel, L. M. Herz, M. B. Johnston, and F. Giustino, *J. Phys. Chem. C* **119**, 25703 (2015).
  - <sup>23</sup> F. Brivio, J. M. Frost, J. M. Skelton, A. J. Jackson, O. J. Weber, M. T. Weller, A. R. Goñi, A. M. A. Leguy, P. R. F. Barnes, and A. Walsh, *Phys. Rev. B* **92**, 144308 (2015).
  - <sup>24</sup> A. Mattoni, A. Filippetti, M. Saba, C. Caddeo, and P. Delugas, *J. Phys. Chem. Lett.* **7**, 529 (2016).
  - <sup>25</sup> T. Hata, G. Giorgi, and K. Yamashita, *Nano Lett.* **16**, 2749 (2016).
  - <sup>26</sup> S.-Y. Yue, X. Zhang, G. Qin, J. Yang, and M. Hu, *Phys. Rev. B* **94**, 115427 (2016).
  - <sup>27</sup> A. J. Neukirch, W. Nie, J.-C. Blancon, K. Appavoo, H. Tsai, M. Y. Sfeir, C. Katan, L. Pedesseau, J. Even, J. J. Crochet, G. Gupta, A. D. Mohite, and S. Tretiak, *Nano Lett.* **16**, 3809 (2016).
  - <sup>28</sup> A. Poglitsch and D. Weber, *J. Chem. Phys.* **87**, 6373 (1987).
  - <sup>29</sup> N. Onoda-Yamamuro, T. Matsuo, and H. Suga, *J. Phys. Chem. Sol.* **51**, 1383 (1990).
  - <sup>30</sup> A. A. Bakulin, O. Selig, H. J. Bakker, Y. L. Rezus, C. Müller, T. Glaser, R. Lovrincic, Z. Sun, Z. Chen, A. Walsh, J. M. Frost, and T. L. C. Jansen, *J. Phys. Chem. Lett.* **6**, 3663 (2015).
  - <sup>31</sup> A. M. A. Leguy, J. M. Frost, A. P. McMahon, V. G. Sakai, W. Kockelmann, C. Law, X. Li, F. Foglia, A. Walsh, B. C. O'Regan, J. Nelson, J. T. Cabral, and P. R. F. Barnes, *Nature Comm.* **6**, 7124 (2015).
  - <sup>32</sup> E. Mosconi, C. Quarti, T. Ivanovska, G. Ruani, and F. De Angelis, *Phys. Chem. Chem. Phys.* **16**, 16137 (2014).
  - <sup>33</sup> J. M. Frost, K. T. Butler, and A. Walsh, *APL Materials* **2**, 081506 (2014).
  - <sup>34</sup> M. A. Carignano, A. Kachmar, and J. Hutter, *J. Phys. Chem. C* **119**, 8991 (2015).
  - <sup>35</sup> C. Goehry, G. A. Nemnes, and A. Manolescu, *J. Phys. Chem. C* **119**, 19674 (2015).
  - <sup>36</sup> S. Meloni, T. Moehl, W. Tress, M. Franckevicius, M. Saliba, Y. H. Lee, P. Gao, M. K. Nazeeruddin, S. M. Zakeeruddin, U. Rothlisberger, and M. Graetzel, *Nature Comm.* **7**, 10334 (2016).
  - <sup>37</sup> J. Even, M. Carignano, and C. Katan, *Nanoscale* **8**, 6222 (2016).
  - <sup>38</sup> A. Mattoni, A. Filippetti, M. I. Saba, and P. Delugas, *J. Phys. Chem. C* **119**, 17421 (2015).
  - <sup>39</sup> J. M. Frost, K. T. Butler, F. Brivio, C. H. Hendon, M. van Schilfgaarde, and A. Walsh, *Nano Lett.* **14**, 2584 (2014).
  - <sup>40</sup> I. Swainson, R. Hammond, C. Soullire, O. Knop, and W. Massa, *J. Solid State Chem.* **176**, 97 (2003).

- <sup>41</sup> L. Chi, I. Swainson, L. Cranswick, J.-H. Her, P. Stephens, and O. Knop, *J. Solid State Chem.* **178**, 1376 (2005).
- <sup>42</sup> T. Baikie, Y. Fang, J. M. Kadro, M. Schreyer, F. Wei, S. G. Mhaisalkar, M. Graetzel, and T. J. White, *J. Mater. Chem. A* **1**, 5628 (2013).
- <sup>43</sup> P. E. Blöchl, *Phys. Rev. B* **50**, 17953 (1994).
- <sup>44</sup> G. Kresse and J. Hafner, *Phys. Rev. B* **47**, 558 (1993).
- <sup>45</sup> G. Kresse and J. Furthmüller, *Phys. Rev. B* **54**, 11169 (1996).
- <sup>46</sup> G. Kresse and D. Joubert, *Phys. Rev. B* **59**, 1758 (1999).
- <sup>47</sup> J. P. Perdew, A. Ruzsinszky, G. I. Csonka, O. A. Vydrov, G. E. Scuseria, L. A. Constantin, X. Zhou, and K. Burke, *Phys. Rev. Lett.* **100**, 136406 (2008).
- <sup>48</sup> M. P. Allen and D. J. Tildesley, *Computer simulation of liquids* (Oxford university press, 1991).
- <sup>49</sup> E. Menéndez-Proupin, P. Palacios, P. Wahnón, and J. C. Conesa, *Phys. Rev. B* **90**, 045207 (2014).
- <sup>50</sup> M. R. Filip, G. E. Eperon, H. J. Snaith, and F. Giustino, *Nature Comm.* **5**, 6757 (2014).
- <sup>51</sup> M. R. Filip and F. Giustino, *Phys. Rev. B* **90**, 245145 (2014).
- <sup>52</sup> C. Quarti, E. Mosconi, and F. D. Angelis, *Chem. Mat.* **26**, 6557 (2014).
- <sup>53</sup> A. Amat, E. Mosconi, E. Ronca, C. Quarti, P. Umari, M. K. Nazeeruddin, M. Grätzel, and F. De Angelis, *Nano Lett.* **14**, 3608 (2014).
- <sup>54</sup> J.-H. Lee, N. C. Bristowe, P. D. Bristowe, and A. K. Cheetham, *Chem. Commun.* **51**, 6434 (2015).
- <sup>55</sup> J. H. Lee, J.-H. Lee, E.-H. Kong, and H. M. Jang, *Sci. Rep.* **6**, 21687 (2016).
- <sup>56</sup> C. Quarti, E. Mosconi, and F. De Angelis, *Phys. Chem. Chem. Phys.* **17**, 9394 (2015).
- <sup>57</sup> C. Quarti, E. Mosconi, J. M. Ball, V. D’Innocenzo, C. Tao, S. Pathak, H. J. Snaith, A. Petrozza, and F. De Angelis, *Energy Environ. Sci.* **9**, 155 (2016).
- <sup>58</sup> C. Motta, F. El-Mellouhi, and S. Sanvito, *Phys. Rev. B* **93**, 235412 (2016).
- <sup>59</sup> J. Li and P. Rinke, *Phys. Rev. B* **94**, 045201 (2016).
- <sup>60</sup> K. Momma and F. Izumi, *J. Appl. Crystallogr* **41**, 653 (2008).